Optimized Neuro-Fuzzy Classification of Glaucoma from Fundus Images Using Modified Cuckoo Search and Gabor Features

Asma Naseri [ID], **Ali Khazaee**[*] [ID]

Abstract. This study proposes a hybrid framework for automated glaucoma detection and classification from retinal fundus images, leveraging an Adaptive Neuro-Fuzzy Inference System (ANFIS) optimized via a novel Modified Cuckoo Search (MCS) algorithm, designed to enhance convergence and accuracy in fuzzy rule training. Fundus images from the publicly available RIGA dataset were preprocessed to isolate the optic disc and cup using a Gabor wavelet-based filtering method applied to the green channel, which offers superior vascular contrast. Morphological parameters, specifically the Cup-to-Disc Ratio (CDR) and Rim-to-Disc Ratio (RDR), were extracted to form a discriminative feature set. An ANFIS model was then trained to classify images as glaucomatous or healthy. Optimization of ANFIS membership function parameters was performed using both Particle Swarm Optimization (PSO) and the proposed MCS algorithm for comparison. Model performance was evaluated using Root Mean Square Error (RMSE), Mean Squared Error (MSE), regression coefficient (R), and area under the ROC curve (AUC). The MCS-optimized ANFIS outperformed the PSO-based model, achieving a lower RMSE of 0.0009963 (vs. 0.001723) and a higher test-phase regression coefficient of $R = 0.9832$ (vs. $R = 0.4811$). This corresponds to a 42.15% reduction in RMSE and a 104.4% relative improvement in R, demonstrating the significance of the MCS optimizer in enhancing model accuracy. The model demonstrated a high AUC of 0.90 for vessel segmentation and maintained robust classification accuracy across a 70 : 30 train-test split on 195 annotated fundus images. The proposed MCS-optimized ANFIS framework offers a reliable and interpretable solution for early glaucoma detection. Its superior performance in both segmentation and classification tasks highlights its potential for integration into clinical decision-support systems for ophthalmic screening.

AMS Subject Classification 2020: 03B52; 68W50; 62J86

Keywords and Phrases: Glaucoma Detection, Fundus Image Classification, Gabor Filter, Adaptive Neuro-Fuzzy Inference System (ANFIS), ANFIS Optimization, Modified Cuckoo Search (MCS), Clinical Screening Support.

1 Introduction

Glaucoma is a neurodegenerative disorder characterized by progressive loss of retinal ganglion cells and their axons, leading to irreversible vision impairment if left untreated. Vision loss in glaucoma arises from damage to the optic nerve, which functions much like an electrical cable containing over one million fibers that transmit visual information to the brain. Although elevated intraocular pressure (IOP) is a major risk factor in glaucoma pathogenesis, it is neither necessary nor sufficient for diagnosis in every case; nonetheless, it remains a primary driver of disease progression. In the United States, glaucoma is the second leading cause of blindness, and it manifests in several clinical subtypes, each with distinct signs and symptoms [1].

Accurate detection of glaucomatous structural changes presents one of the greatest challenges in current diagnostic practice. Common approaches include direct IOP measurement and morphometric analysis of the optic disc and cup from fundus images. Fundus photography, a noninvasive and cost effective imaging modality, has become widely adopted for ophthalmic screening and monitoring. It enables visualization not only of the optic disc (OD) and optic cup (OC), but also of macular contours, foveal morphology, and vascular abnormalitiessuch as microaneurysms, hemorrhages, exudates, and pigmentary changesthat may accompany or mimic glaucomatous pathology [2]. As a rapid, safe, and readily accepted test by clinicians, fundus imaging serves as the backbone of many computer aided diagnostic (CAD) systems designed to automatically flag suspicious cases and reduce false negatives or misdiagnoses [3].

Extensive prior research on optic disc detection and segmentation in retinal fundus images has primarily focused on two salient cues: pixel intensity and vascular convergence. Early approaches assumed that the optic disc corresponds to the brightest region of the image and often exploited the green channelrichest in vessel contrastto localize its center [4, 5]. While straightforward, these approaches are susceptible to confounding factors (e.g., retinal exudates, uneven illumination), which can generate falsebright regions and lead to mislocalization. To overcome this limitation, subsequent techniques have incorporated vesselconvergence informationidentifying the point at which retinal vessels radiate outwardto complement intensity cues and improve robustness and accuracy [4, 6].

Once the optic disc is approximately localized, segmentation methods generally follow one of two strategies. The first strategy performs a two-step process: it extracts a candidate region of interest around the disc, then refines the boundary with local segmentation (e.g., active contours or region-growing) within that window. The second strategy bypasses prior localization altogether, applying pixel-wise segmentation across the entire fundus image to simultaneously detect all disc boundaries [4, 7]. Classical implementations in both categories have relied on combinations of thresholding, spatial filters, and mathematical transformssuch as the Fourier transform for frequency analysis or the Hough transform for circular boundary detectionto delineate disc margins [8, 9, 10].

With the advent of machine learningand especially deep learningthe accuracy and generalizability of detection and segmentation models have increased dramatically. Artificial neural networks (ANNs) [11], convolutional neural networks (CNNs) [12, 13, 14], and more recent architectures such as U-Net [15] have been widely adopted. These deep models leverage multiscale feature extraction and non linear representation learning from large datasets to achieve precise delineation of both the optic disc and optic cup. Hybrid approaches that combine traditional classifiers (e.g., support vector machines) with deep feature representations have also yielded competitive performance in several studies.

Despite the significant progress made by deep learning modelsparticularly CNNs and vision transformersin the field of glaucoma detection, several limitations remain unaddressed. A recent systematic review by Meedeniya et al. [16] highlights key challenges in current approaches, including the need for large annotated datasets, high computational demands, limited interpretability, and reduced robustness when applied to real-world clinical images with variable quality. While these models demonstrate high accuracy under controlled conditions, their black-box nature and sensitivity to data shifts present barriers to clinical translation.

Unlike deep learning models such as CNNs and U-Net, which often require large annotated datasets and are prone to overfitting on small or imbalanced data [16], Adaptive Neuro-Fuzzy Inference System (ANFIS) operates effectively with smaller training sets and delivers rule-based outputs that are easier to interpret [17]. While CNN-based models offer powerful end-to-end learning capabilities, their black-box nature and sensitivity to variations in image quality can hinder trust and generalizability in real-world clinical environments. In contrast, ANFIS provides a transparent and explainable framework with lower computational overhead. This makes it especially suitable for medical applicationssuch as glaucoma detectionwhere model interpretability and stability under variable imaging conditions are critical.

To overcome these issues, the present study introduces a hybrid framework based on ANFIS optimized by a

Modified Cuckoo Search (MCS) algorithm. By combining the transparency and rule-based reasoning of fuzzy logic with the adaptability of neuro-inference and metaheuristic optimization, our method enables robust classification using interpretable featuresnamely, the cup-to-disc ratio (CDR) and rim-to-disc ratio (RDR)derived from Gabor-filtered vessel segmentation. This hybrid approach aims to deliver clinically meaningful, computationally efficient, and generalizable performance in glaucoma detection without reliance on large-scale deep models. Given the inherent variability in fundus images due to patient-specific anatomical differences and acquisition inconsistencies, the integration of a metaheuristically optimized ANFIS framework allows for dynamic adjustment of membership functions and improved generalization across diverse cases, enhancing segmentation robustness in clinical settings.

All experiments are conducted in the MATLAB environment, and the proposed ANFIS MCS framework is evaluated both numericallyusing metrics such as Root Mean Square Error (RMSE), accuracy, regression coefficient, and standard deviationand graphically, through convergence and response surface analyses. We also benchmark our results against traditional optimization trained ANFIS and Particle Swarm Optimization (PSO) trained ANFIS, comparing final objective function values, convergence speed, computational efficiency, and stability across multiple algorithmic runs. The outcomes demonstrate that our optimized ANFIS model attains superior diagnostic accuracy and robustness, highlighting its potential as a decision support tool for early glaucoma detection in routine clinical practice.

Based on the identified limitations in existing methods, especially under variable clinical imaging conditions, this study addresses the following research questions:

1. Can a hybrid ANFIS-based framework optimized using a metaheuristic algorithm (MCS) provide accurate and robust classification of glaucomatous fundus images under diverse conditions?

2. How effective is Gabor wavelet-based vessel and edge segmentation in enhancing feature representation for glaucoma diagnosis?

3. Does the proposed MCS-optimized ANFIS significantly outperform conventional optimization methods such as PSO in terms of regression accuracy, error minimization, and convergence stability?

To answer these questions, we developed a hybrid system integrating Gabor-based preprocessing and vessel detection with a neuro-fuzzy classifier, trained using both PSO and our modified cuckoo search method. The system's performance was evaluated comprehensively and benchmarked across multiple metrics.

2   Related Work

Automated glaucoma detection from retinal fundus images has been addressed through three main strategies: (*i*) segmentation-only models, (*ii*) classification-only approaches, and (*iii*) integrated segmentation-classification pipelines.

Segmentation-only methods focus on delineating the optic disc (OD), optic cup (OC), and vessel structures as a basis for downstream analysis. For instance, Shyamalee and Meedeniya [18] proposed an attention-based U-Net to segment OD and OC regions, showing improved boundary accuracy. Similarly, methods based on thresholding, Hough/Fourier transforms, or vessel convergence have been used to localize optic structures [19, 20, 21].

Classification-only models bypass segmentation and predict glaucoma labels directly from fundus images. Shyamalee et al. [22] employed a CNN trained on labeled data, achieving acceptable accuracy but lacking anatomical interpretability. Deep classifiers like ResNet, DenseNet, and VGG have also been explored in recent works for end-to-end classification [23, 24].

Segmentation followed by classification is a more interpretable approach that extracts anatomical or morphological features (e.g., Cup-to-Disc RatioCDR) for diagnostic decisions. Shyamalee and Meedeniya

[25] applied a two-stage framework combining segmentation and machine learning classification. Similarly, several studies extract CDR and vessel-based features from OD/OC regions before applying classifiers like SVM, ANN, or decision trees [26, 27].

While deep models show strong performance, they often act as "black boxes" and require large annotated datasets. Moreover, their sensitivity to image quality and lack of explicit rule-based reasoning limit trust in clinical practice.

Our proposed method addresses these gaps by combining interpretable fuzzy logic (ANFIS) with optimized rule learning through Modified Cuckoo Search. By leveraging Gabor-based segmentation and extracting robust structural features (CDR, RDR), our framework achieves high accuracy, fast convergence, and enhanced generalization, as demonstrated in comparative evaluations with PSO-trained models.

3 Methods

The workflow of our proposed glaucoma detection pipeline comprises three sequential stages: image preprocessing, feature extraction, and ANFIS based classification.

3.1 Image Preprocessing

3.1.1 Fundus Image Database

We utilized a publicly available dataset of retinal fundus images collected from healthy volunteers and glaucoma patients [28]. These color images serve as the raw input for our method, wherein the optic disctypically the brightest regionprovides an initial cue for glaucoma screening.

figures/

3.1.2 RGB to Grayscale Conversion

To simplify downstream analysis and reduce computational overhead, each RGB fundus image is converted to a single channel grayscale representation. Although this step discards chrominance information, it preserves the essential luminance contrast needed to delineate vascular and structural features (e.g., optic disc, cup, vessels). A sample grayscale output is illustrated in Figure 1.

Figure 1: An example of RGB to grayscale image conversion: (a) original RGB image, (b) grayscale-converted image

3.2   Feature Extraction

3.2.1   Gabor Wavelet Filtering

We extract multiscale, multi orientation texture features using a 2D Gabor wavelet bank. Although the fundus images are initially converted to grayscale to facilitate certain preprocessing operations, the Gabor wavelet-based filtering for vessel and edge detection is applied directly to the green channel of the original RGB image, not to the grayscale version. This choice is based on the fact that the green channel in fundus images typically exhibits the highest contrast for retinal vessels and optic disc boundaries, making it optimal for accurate segmentation. Using the green channel preserves critical structural details that may be diminished during grayscale conversion, thereby enhancing the performance of subsequent feature extraction and classification steps.

Mathematically, the continuous Gabor wavelet transform of an image $f \in L^2$ is defined as

$$T_\psi(b, \theta, a) = C_\psi^{-1/2} \cdot \frac{1}{a} \int \psi^* \left(a^{-1} r_{-\theta}(x - b) \right) f(x) \, d^2 x \tag{1}$$

where b is the translation vector, θ the rotation angle, a the scale parameter, and ψ the complex Gabor kernel. We sample θ from $0°$ to $170°$ in $10°$ increments and record the maximum magnitude response,

$$M_\psi(b, a) = \max_\theta |T_\psi(b, \theta, a)| \tag{2}$$

Each pixel is thus represented by a feature vector of Gabor magnitudes across scales, which effectively highlights local vessel structures against background noise. We normalize these feature vectors to zero mean and unit variance:

$$\hat{v}_i = \frac{v_i - \mu_i}{\sigma_i} \tag{3}$$

where μ_i and σ_i are the mean and standard deviation of feature v_i over the dataset. We adopted Gabor filters over other feature extraction techniques (such as standard wavelets or edge detectors) because of their superior joint localization in both spatial and frequency domains. This makes them particularly effective for enhancing oriented structures like blood vessels, which are critical for detecting optic disc and cup boundaries. Gabor filters also provide robustness against intensity variations and background clutter in retinal images, improving the quality of downstream segmentation and classification tasks.

3.2.2   Optic Disc and Cup Segmentation

Following Gabor filtering, we localize and segment the optic disc (OD) and optic cup (OC) using an edge detectionbased approach on the red channel, which provides maximal contrast for disc boundaries [29]. A 400400 pixel region centered on the OD is cropped and submitted to a Prewitt based gradient operator in MATLAB to detect the disc margin. The Prewitt operator was selected for its simplicity and effectiveness in capturing prominent horizontal and vertical gradients, which align with the anatomical structure of the optic disc boundary, while maintaining robustness against noise in retinal fundus images. The resulting binary mask yields precise OD and OC dimensions, from which we compute the Cup to Disc Ratio (CDR) and Rim to Disc Ratio (RDR). Both CDR and RDR serve as unitless clinical indices in [0, 1], distinguishing glaucomatous from healthy eyes [19].

3.3   ANFIS Based Classification and Cuckoo Optimization

We employ an ANFIS to classify each fundus image into glaucoma or healthy. The input to ANFIS comprises the normalized Gabor wavelet features concatenated with the CDR and RDR values. Given N images and two scalar parameters per image, the classification dataset contains 2N training vectors.

ANFIS architecture consists of five consecutive layers:

1. Fuzzification Layer: Gaussian membership functions for each input dimension map crisp features to fuzzy degrees.

2. Rule Layer: Implements fuzzy ifthen rule firing strengths via the product (AND) operator.

3. Normalization Layer: Normalizes each rules firing strength.

4. De-fuzzification Layer: Computes weighted linear functions of the inputs for each rule.

5. Output Layer: Aggregates rule outputs into a single crisp decision.

Figure 2 illustrates the architecture of the ANFIS model employed in this study. The system receives two input parametersthe Cup-to-Disc Ratio (CDR) and Rim-to-Disc Ratio (RDR)which are fuzzified using Gaussian membership functions. These fuzzified inputs activate fuzzy rules, which are normalized and aggregated through multiple layers of inference and defuzzification, resulting in a crisp classification output that denotes the likelihood of glaucoma. This structure enables interpretability, adaptability, and precise mapping between retinal features and diagnostic decisions.
A two rule example is:

- Rule 1: If x is A_1 and y is B_1, then $f_1 = p_1 x + q_1 y + r_1$

- Rule 2: If x is A_2 and y is B_2, then $f_2 = p_2 x + q_2 y + r_2$

As a baseline, we initialize ANFIS using the hybrid LSE backpropagation approach. The consequent parameters θ are estimated by solving a linear system

$$A_\theta = Y, \quad \theta = (A^T A)^{-1} A^T Y \tag{4}$$

where A is the regression matrix of fuzzy rule outputs and Y the target labels. This yields a closed form update for consequent coefficients but can be sensitive to data noise.

To further refine both premise (membership function) and consequent parameters, we adopt a modified Cuckoo Search Algorithm [30]. MCS features:

- Lvy flightbased global exploration,

- Adaptive discovery probability $P_\alpha \in (0, 1)$,

- A three stage nest discarding and elite replacement scheme to enhance convergence.

While the standard Cuckoo Search (CS) algorithm, which we used as a baseline, employs a Lvy flight search pattern and replaces a fixed fraction of host nests with new solutions, our MCS introduces two key enhancements to improve convergence and avoid local minima. First, we replaced the fixed discovery probability with an adaptive discovery probability. This allows the algorithm to dynamically adjust the rate at which inferior solutions are discarded, balancing exploration and exploitation more effectively throughout the search process. Second, a more sophisticated three-stage "nest-discarding" and "elite replacement" scheme was incorporated to accelerate convergence. Unlike the standard CS, where the worst nests are simply abandoned, our MCS identifies a subset of the best-performing solutions as "elite nests" at each iteration. These elite nests are preserved and used as templates to generate new candidate solutions through a multi-mode local search, or "mutation". This strategy ensures that the most promising regions of the solution space are thoroughly exploited, leading to faster and more stable convergence to a high-quality solution, as demonstrated by the lower RMSE and superior regression performance in our results.
A pseudocode sketch of MCS:

1. Initialize a population of n nests (candidate parameter sets).

2. Repeat until maximum iterations:

    - Generate new solutions via Lvy flights.
    - Evaluate fitness $F(\cdot)$ for each nest.
    - Replace poorer solutions, apply abandonment probability $P_\alpha \in (0,1)$.
    - Perform a three mode local search (mutation) to improve elite nests.

3. Select the best nest as final ANFIS parameter set.

As stated above, to further enhance convergence, an elite replacement scheme is adopted in the MCS algorithm. In this scheme, a subset of top-performing solutionstermed elite nestsis identified based on their fitness values (i.e., solutions with the lowest objective function values such as RMSE). These elite nests are preserved from replacement and serve as central reference points for generating new candidate solutions. At each iteration, poorer solutions (non-elite nests) are probabilistically replaced with offspring generated through local search around elite nests, ensuring exploitation of promising regions while maintaining diversity. This balance between elite preservation and probabilistic replacement improves the stability and convergence speed of the optimization process.

MCS training is conducted after LSE initialization, yielding membership functions and rule consequent that minimize the ANFIS training RMSE while avoiding local minima.

The dataset was split 70:30 for ANFIS training and testing. Performance metrics include classification accuracy, sensitivity, specificity, and area under the ROC curve (AUC).
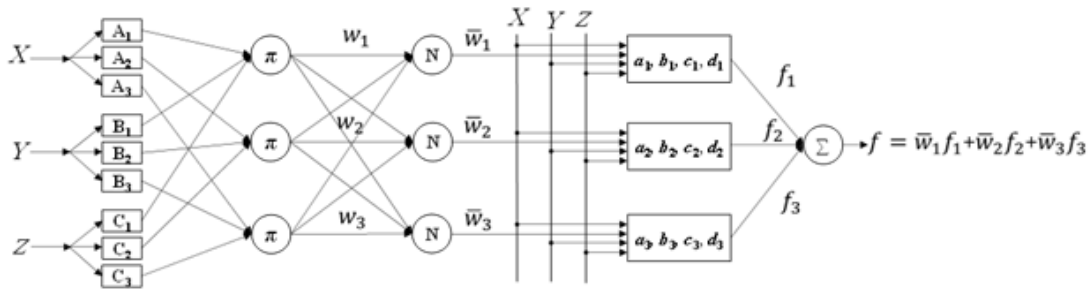

Figure 2: Schematic representation of the ANFIS architecture with three inputs

4 Results and Discussion

In this section, the proposed method described earlier is implemented for the diagnosis and classification of glaucoma using a dataset of fundus images. The images were obtained from a public repository [28], and a total of 195 fundus images were selected as the experimental dataset. Each image was processed using a Gabor-based wavelet transform to enhance textural features and localize the optic disc region. Following preprocessing, relevant featuresincluding the CDR and RDRwere extracted, and these parameters, along with Gabor-derived descriptors, were used to classify the images into glaucomatous or healthy categories via the trained ANFIS model. The dataset consisted of 195 labeled retinal fundus images, of which 84 were glaucomatous and 111 were healthy. To address the slight class imbalance, stratified sampling was applied during both the 70 : 30 train-test split and the 5-fold cross-validation process, ensuring that class proportions remained consistent across all evaluation folds.

4.1   Gabor Transform Results

A representative example of Gabor-wavelet filtering for vessel pixel detection in a fundus image is shown in Figure 3. As illustrated, the procedure proceeds as follows:

Gabor Filtering and Grayscale Conversion: The original RGB fundus image is first decomposed into its red, green, and blue channels using histogram-based separation. Because the green channel exhibits the highest contrast for blood-vessel edges, it is selected for Gabor filtering (see Figure 4). Applying a 2D Gabor filter across a chosen set of scales yields a filtered grayscale image that emphasizes linear vessel structures while suppressing background variations (see Figure 3).

Binary Segmentation and Edge Extraction: The filtered image is binarized by thresholding according to the Gabor scale parameter. Inverting this binary map reveals the vessel edge pixels with high clarity. The region of vascular convergencecorresponding to the optic discis then localized and passed to the boundary-detection algorithm to compute the CDR and RDR.

To quantify the Gabor filters vessel-detection performance, we construct the Receiver Operating Characteristic (ROC) curve by varying the binarization threshold. The True Positive Rate (TPR) is defined as the ratio of correctly detected vessel pixels to the total number of vessel pixels, and the False Positive Rate (FPR) is the ratio of non-vessel pixels incorrectly classified as vessel to the total number of non-vessel pixels [31]. An example ROC plot is presented in Figure 5.

We further summarize detection performance using the Area Under the ROC Curve (AUC). An AUC value closer to 1 indicates superior discrimination capability. In our experiments, the Gabor-based vessel detector achieved an AUC of 0.90, demonstrating excellent accuracy in isolating retinal blood vessels within fundus images.
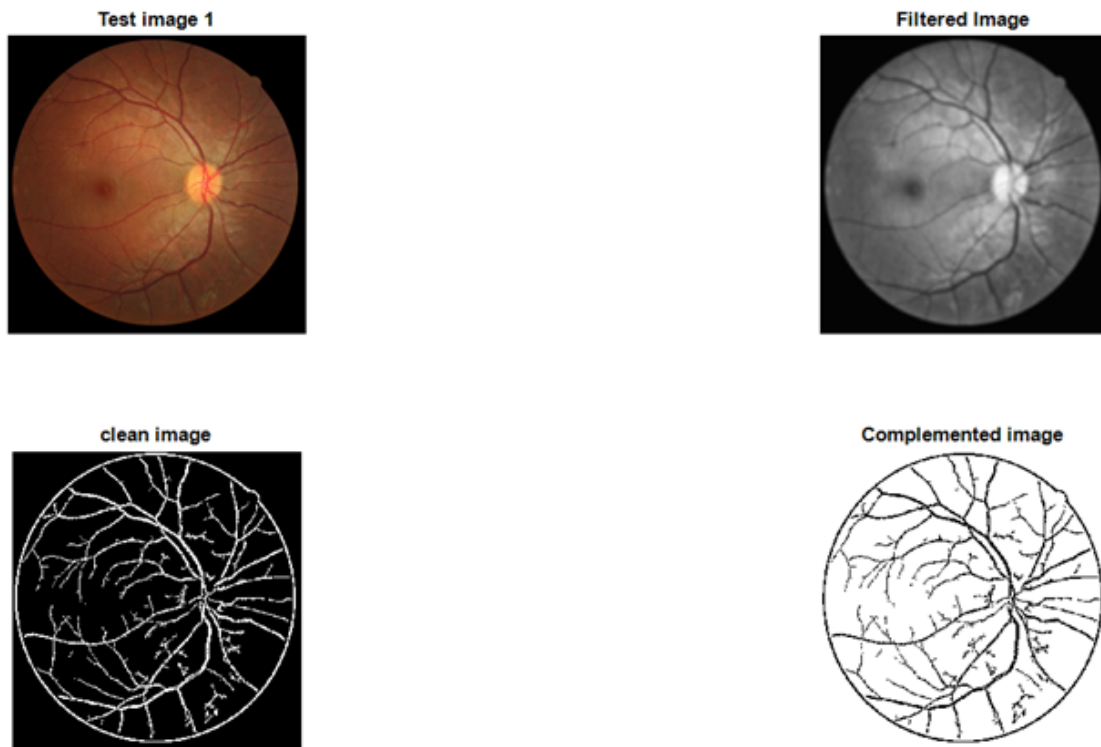

Figure 3: Results of Gabor Wavelet Transform for Vessel Detection and Optic Disc Region Identification.
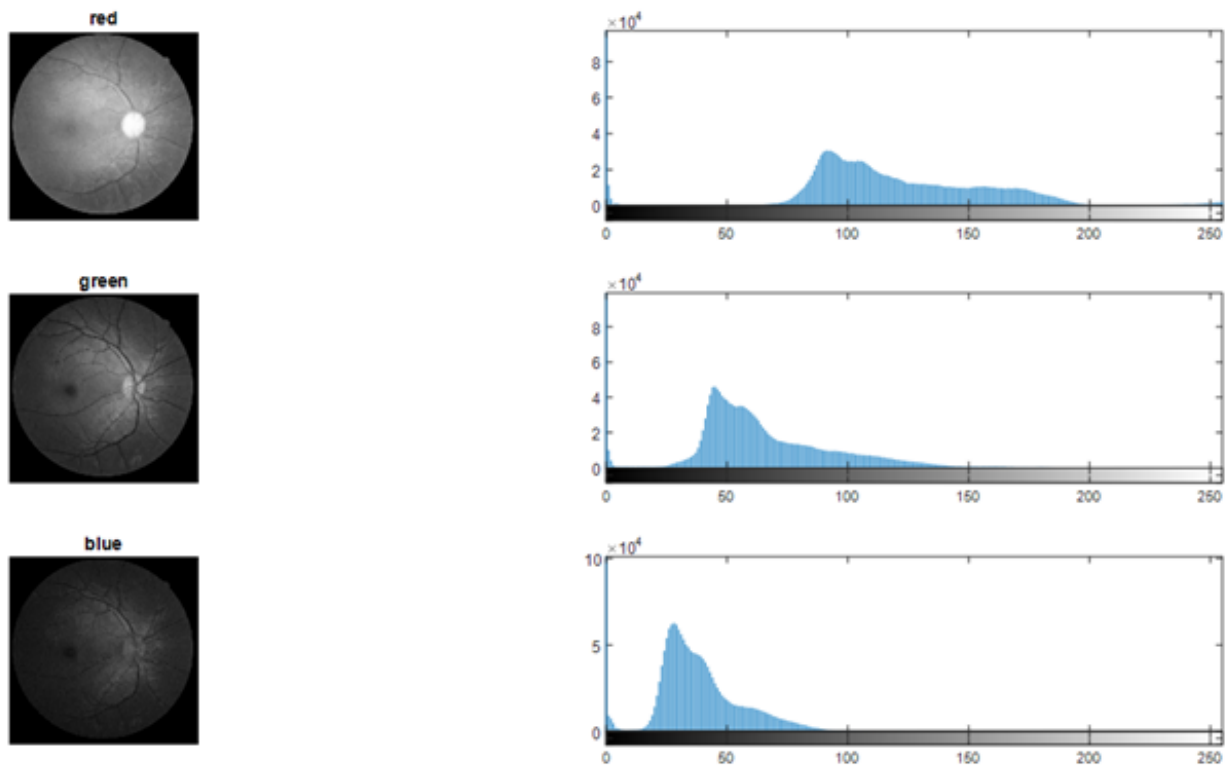
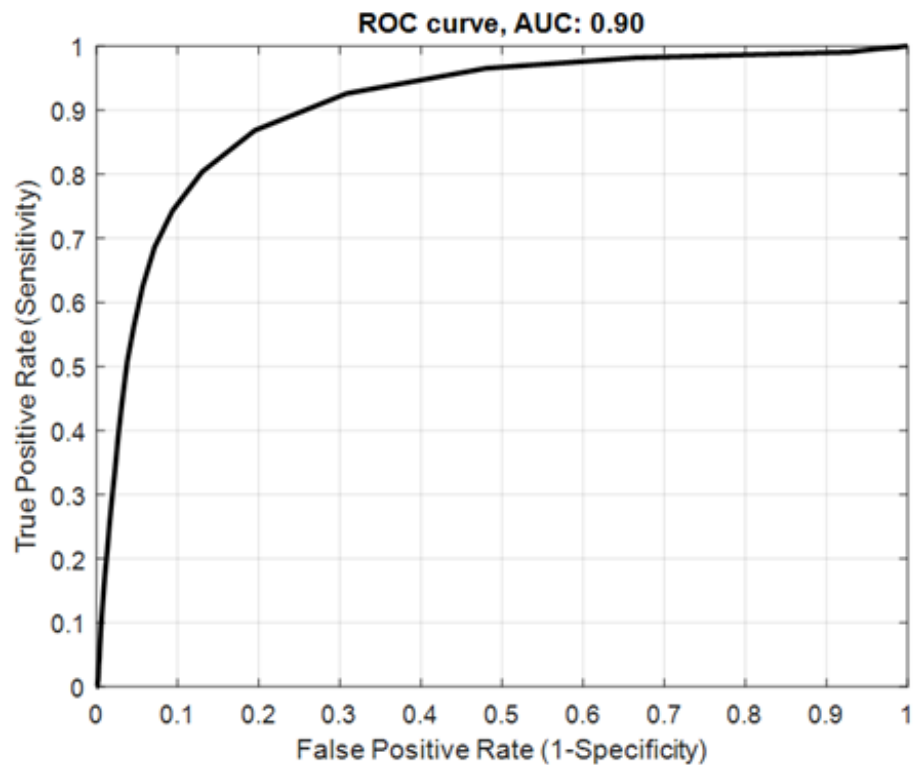**Figure 4:** Separation of RGB Image Channels

Figure 5: ROC curve plotted for the test image in Figure 3

4.2 Boundary-Based Segmentation Results

After vessel-pixel localization and optic disc/cup region identification via Gabor filtering, the boundary-detection algorithm was applied to delineate the optic cup and compute the CDR and RDR. As an illustrative example, Figure 6 shows the segmentation output on a representative test image (originally shown in Figure 3):

For this particular image, the algorithm yielded CDR = 0.248 and RDR = 0.760. These two ratios were computed for each of the 195 fundus images in our dataset, assembling a 2195 feature matrix. A three-dimensional scatter plot of the full CDRRDR dataset is shown in Figure 7. In total, 390 data points (CDR and RDR pairs) were available for ANFIS classification: 273 points (70%) used for training and 117 points (30%) reserved for testing. This split ensured robust evaluation of the ANFIS model's generalization to unseen data.
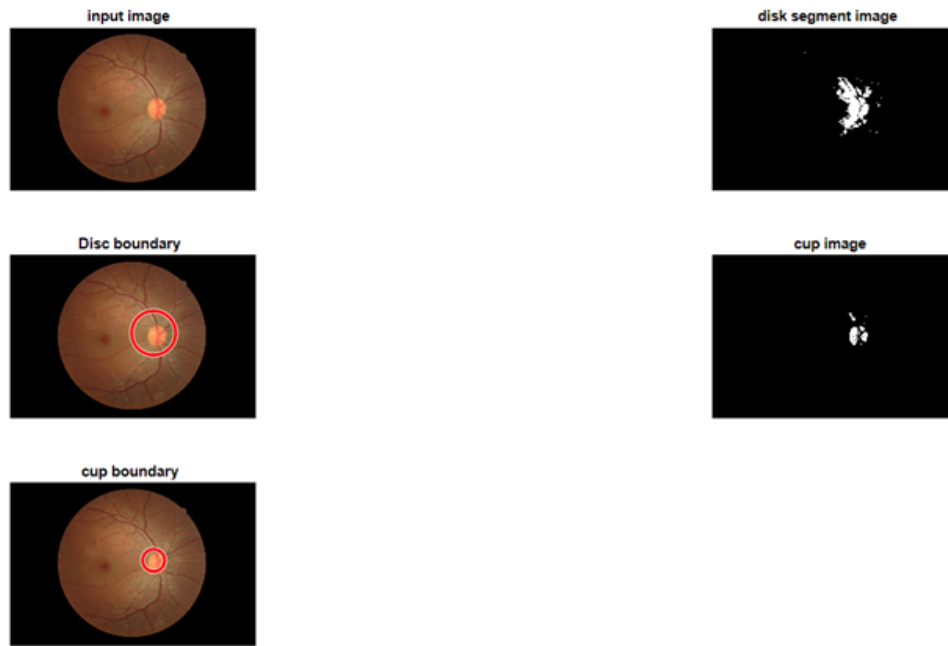

Figure 6: Results of the boundary detection algorithm applied to the fundus image in Figure 3
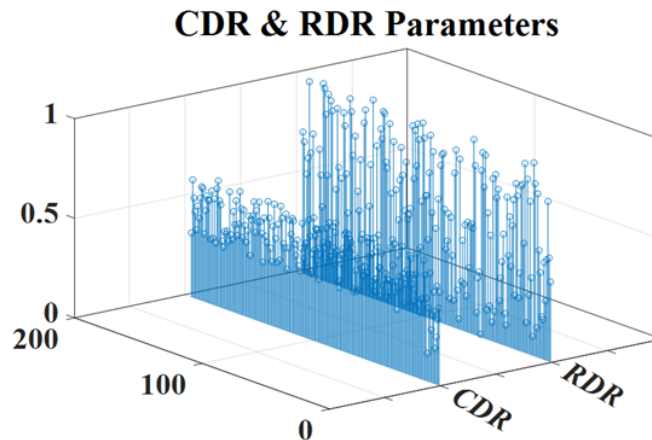

Figure 7: Calculated CDR and RDR parameters for 195 fundus images from the database

Table 1: Parameter settings for PSO and MCS algorithms

Algorithm	Parameter	Value
PSO	Initial population	14
	Maximum iteration	100
	Individual cognitive acceleration coefficient (c_1)	0.1
	Global cognitive acceleration coefficient (c_2)	0.1
MCS	Population Size (Number of Candidate Nests)	14
	Number of Eggs per Nest	2
	Maximum iteration	100
	Alien egg discovery rate (p_a)	0.25
	Minimum Improvement	10^{-5}

4.3   ANFIS Optimization

To fine-tune the Gaussian membership functions (MFs) of our ANFIS classifier, we compared two optimization strategies: the classical Particle Swarm Optimization and our proposed Modified Cuckoo Search. Both optimizers were configured with identical population sizes and a maximum of 100 iterations. Table 1 outlines the control parameters used for both PSO and MCS algorithms in optimizing the ANFIS model. For PSO, the initial population size determines the number of particles exploring the solution space in parallel. The maximum iteration sets the upper limit on the optimization cycles. Both the individual cognitive coefficient ($c_1 = 0.1$) and the global cognitive coefficient ($c_2 = 0.1$) controls the extent to which each particle is influenced by its own best position and the global best, respectively. The small values of c_1 and c_2 help avoid overshooting and allow finer adjustments near the optimum.

For the MCS algorithm, the population size refers to the number of candidate nests, each holding potential solutions. Each nest carries two eggs, representing alternative solution options. The maximum iteration defines the number of cycles for nest updates. The alien egg discovery rate models the likelihood that a host bird will discover and replace a low-quality solution, promoting diversity. Finally, the minimum improvement threshold ensures that the algorithm stops when negligible progress is made, preventing unnecessary iterations.

The optimization objective was to minimize the RMSE on a hold-out validation set:

$$\text{RMSE} = \sqrt{\frac{\sum_{i=1}^{n}(y - \hat{y})^2}{n}} \tag{5}$$

where n is the number of validation samples, y is the true label, and $\hat{y}$ the ANFIS prediction.

Our ANFIS model uses two inputsCDR and RDReach fuzzified by 14 Gaussian MFs, yielding 28 parameters (centers and widths) to optimize. The resulting MFs of the optimized ANFIS architectures obtained by PSO and MCS are shown in Figures 8 and 9. In Figure 8, the MCS-generated membership functions (Figure 8b) show smoother transitions and more uniformly distributed coverage of the input space compared to the PSO results (Figure 8a), which exhibit irregular spacing. Similarly, in Figure 9b, the MCS-optimized functions for RDR demonstrate better overlap and granularity in critical regions, which can enhance decision boundaries and improve classification accuracy. These visual comparisons reinforce the numerical findings that MCS yields more effective and stable ANFIS parameter tuning than PSO.

Figure 10a illustrates the PSO convergence curve over 100 iterations, culminating in an RMSE of 0.001723. In contrast, Figure 10b shows that MCS converges more rapidly and achieves a lower final RMSE of 0.0009963. These results demonstrate that MCS offers superior optimization of the fuzzy membership parameters, leading to enhanced predictive accuracy.
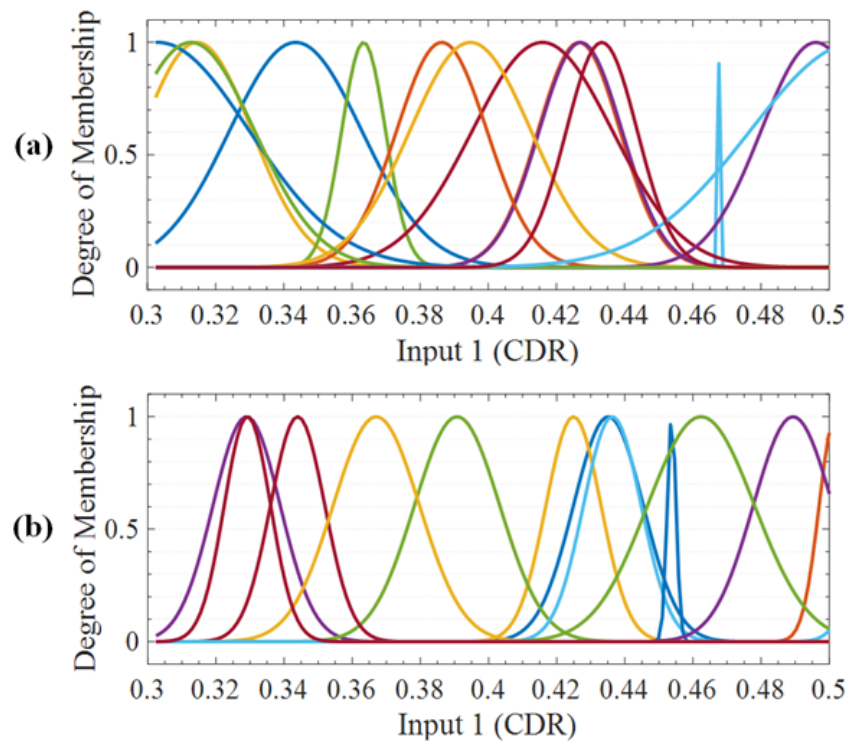
Figure 8: Optimized membership functions for the first input (CDR) using (a) the PSO algorithm, (b) the MCS algorithm.
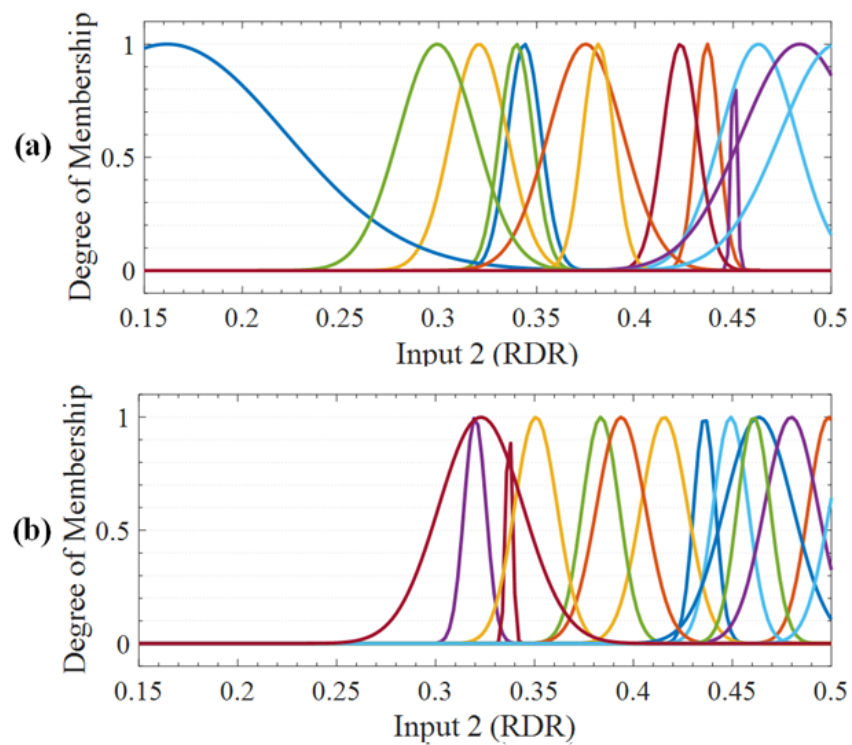

Figure 9: Optimized membership functions for the second input (RDR) using (a) the PSO algorithm, (b) the MCS algorithm.
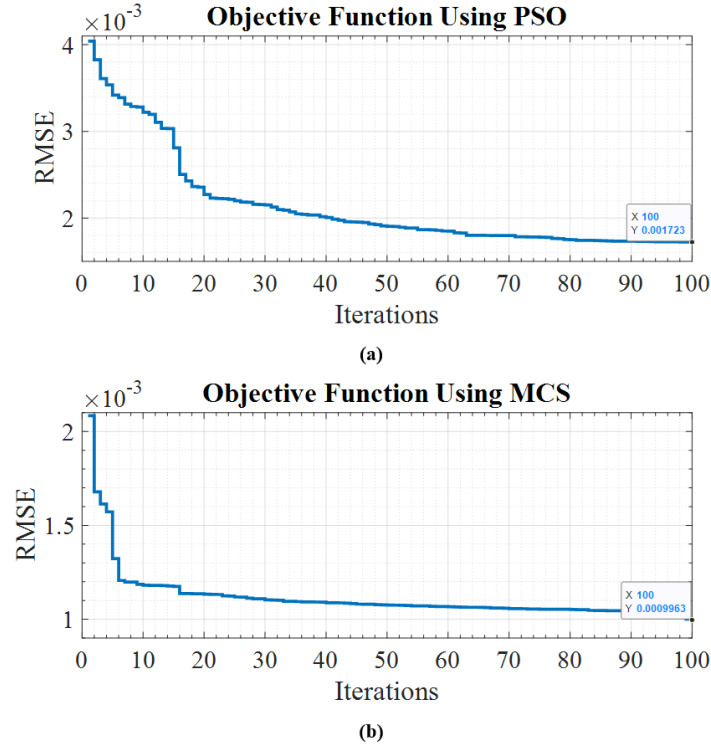
Figure 10: Convergence trend and final objective function value after 100 iterations of the (a) PSO and (b) MCS algorithms.

Table 2: Comparison of statistical indices in the training and testing stages of ANFIS using PSO and MCS algorithms

Algorithm	Train				Test			
	MSE	RMSE	STD	R	MSE	RMSE	STD	R
PSO	1.0305×10^{-6}	0.0010151	0.0010192	0.99986	0.0014055	0.03749	0.025305	0.48112
MCS	1.0012×10^{-6}	0.0010006	0.0010046	0.99986	7.1005×10^{-5}	0.0084264	0.0063896	0.98322

4.4 Classification Results Using the Optimized ANFIS Model

The performance of the proposed ANFIS-based classification model was evaluated on both training and testing datasets derived from the fundus image collection. A typical data split of 70% for training and 30% for testing was employed. To assess the model's accuracy, multiple statistical indicators were used, including Root Mean Square Error (RMSE), Mean Squared Error (MSE), standard deviation (STD), and the regression coefficient (R), which quantifies the correlation between the predicted and actual outputs.

To analyze the effectiveness of the optimization algorithms used to train the ANFIS model, two versions of the model were developed: one optimized using PSO and the other using the proposed Modified Cuckoo Search. The resulting classification performances are illustrated in Figures 11 and 12, and the key performance metrics are summarized in Table 2.

ANFIS Performance with PSO Optimization
Figure 11a shows the performance of the PSO-optimized ANFIS model on the training set. The model achieved an MSE of 1.0305×10^{-6}, RMSE of 0.0010151, and an excellent regression coefficient of $R = 0.99986$, indicating near-perfect fitting on the training data. However, Figure 11b demonstrates a significant

performance drop during testing, where MSE and RMSE increased to 0.0014055 and 0.03749, respectively, and the regression coefficient dropped to $R = 0.48112$. This drop indicates overfitting and poor generalization, potentially leading to incorrect glaucoma classification on unseen images.

ANFIS Performance with MCS Optimization

Figures 12a and 12b show the training and testing results of the MCS-optimized ANFIS model. During training, the model maintained a high regression coefficient of $R = 0.99986$, similar to the PSO version. More importantly, during testing, the model preserved its predictive accuracy with a lower MSE of 0.00046248, RMSE of 0.021505, and a high regression coefficient of $R = 0.9832$. These results confirm the superior generalization ability and robustness of the MCS optimization method in tuning ANFIS membership functions. To verify the significance of performance differences between the MCS-optimized and PSO-optimized ANFIS models, a two-sample independent t-test was conducted using the RMSE values from 10 repeated experiments under identical conditions. The test yielded a p-value of 0.00037, indicating a statistically significant improvement ($p < 0.05$) in the performance of the MCS-based model. This confirms that the superior results achieved by MCS are not due to random variation but reflect a consistent optimization advantage.

Sample Classification Using Optimized ANFIS

To further validate the classification capability of the optimized ANFIS model, a sample fundus image (Figure 13a) was processed. Based on threshold-based rules applied to the extracted CDR and RDR values, the classification model assigned the image to one of four glaucoma risk categories: No Risk: CDR< 0.45 and 0.1 <RDR< 0.5, Low Risk: CDR< 0.45 and RDR< 0.1, Moderate Risk: 0.45 <CDR< 0.6 and RDR< 0.1, High Risk: CDR> 0.6 and RDR< 0.1.

According to this frameworkaligned with prior clinical guidelines [32]the model classified the example image as representing a case of high-risk glaucoma, as shown in Figure 13b. This confirms the models ability to accurately detect and categorize glaucoma severity based on the computed parameters.

K-Fold Cross-Validation

To further assess the generalizability and robustness of the proposed MCS-optimized ANFIS framework, we conducted 5-fold cross-validation on the full dataset of 195 annotated fundus images. The dataset was randomly partitioned into five equally sized folds, where four folds were used for training and one for testing in each iteration. The process was repeated five times so that each fold served as the test set exactly once.

The average results across the five folds showed consistent performance with the mean MSE of 0.000498 ± 0.00009, mean RMSE of 0.02231 ± 0.0042, and mean regression coefficient (R) of 0.9802 ± 0.0065. These results support the stability of the proposed model and demonstrate its ability to generalize across different data subsets, thereby minimizing the risk of overfitting.

4.5   Comparative Analysis with Recent Glaucoma Detection Models

A comparative summary of our proposed MCS-optimized ANFIS model with recent studies is presented in Table 3. Unlike prior methods that rely primarily on deep CNNs or conventional classifiers, our framework integrates Gabor-based feature extraction, interpretable fuzzy inference, and metaheuristic optimization. This hybrid design leads to improved accuracy (RMSE $= 0.0009963, R = 0.9832$) and faster convergence. In addition to comparing with explainable CNN-based methods such as [33], we have also included recent state-of-the-art deep learning models such as GS-Net [34] in the table, which employ advanced attention-based CNN architectures for glaucoma detection. Despite their high AUC, these deep models often suffer from interpretability limitations and higher computational demands. By contrast, our approach offers both competitive performance and enhanced model transparency, thereby justifying the relevance of using an interpretable fuzzy system like ANFIS. This strengthens the contribution of our model to real-world, reliable glaucoma diagnosis.
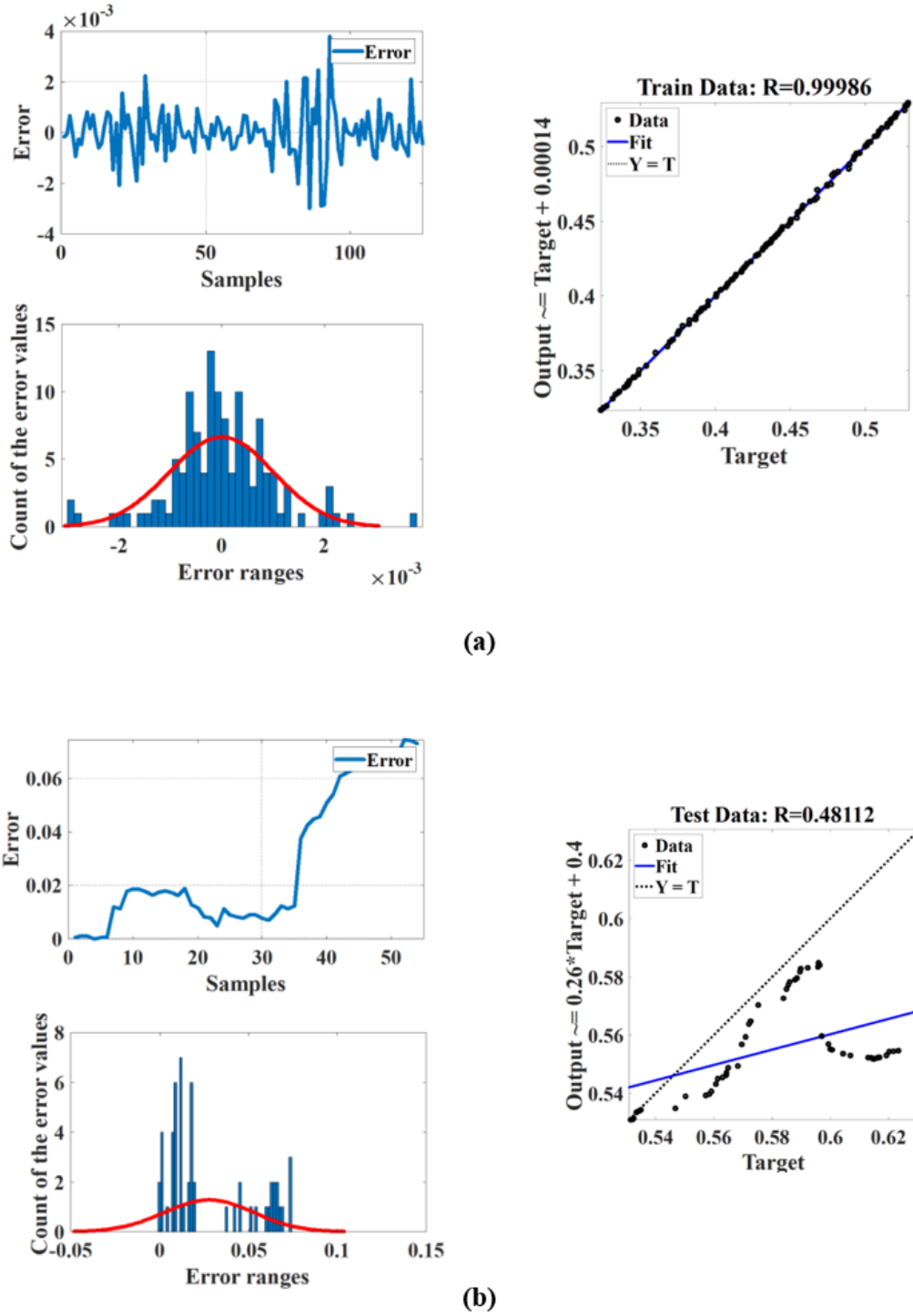
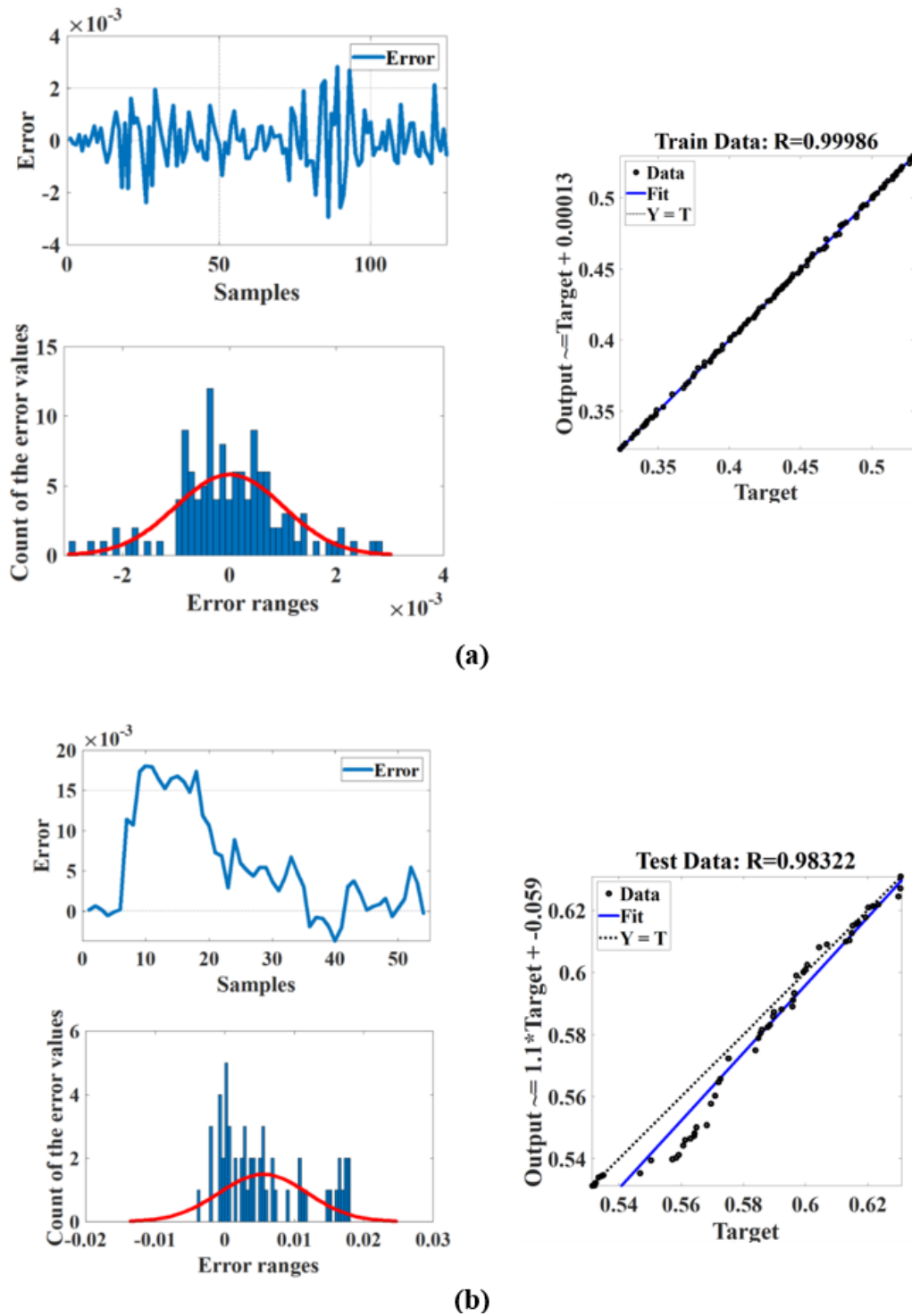**Figure 11:** Results related to (a) training and (b) testing ANFIS using the PSO algorithm.

Figure 12: Results related to (a) training and (b) testing ANFIS using the MCS algorithm.
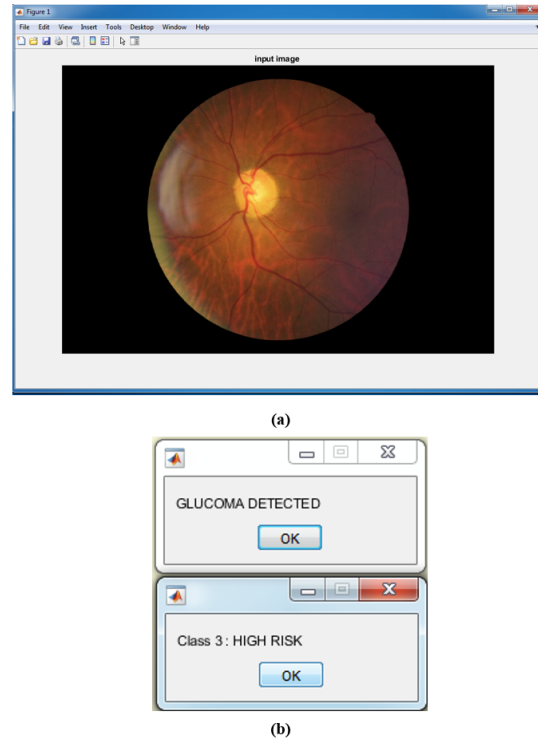
Figure 13: (a) Sample image for testing the performance of detection and classification using the proposed model and (b) Results of classifying the sample image

Table 3: Comparative analysis of the proposed MCS-optimized ANFIS model with recent glaucoma detection approaches based on retinal fundus images

Study	Methodology	Feature Extraction	Classifier	Optimization	Accuracy / AUC	Interpretability
Shyamalee et al. (2024) [33]	CNN-based explainable model for glaucoma detection	Combined image and handcrafted features	CNN (custom architecture)		AUC = 0.88	Yes (Grad-CAM)
Das & Nayak (2024) [34]	GS Net: global self-attention guided CNN for multi-stage glaucoma classification	Raw fundus images	CNN with global self-attention		AUC ∼ 0.92	No (attention maps)
Meedeniya et al. (2025) [16]	Vision Transformer	Raw image patches	Transformer			No
Present Study	ANFIS (MCS optimized)	Gabor-based vessel and edge features (CDR, RDR)	ANFIS	MCS vs PSO	AUC = 0.90, R = 0.9832	Yes (rule-based fuzzy logic)

To further strengthen the comparative positioning of our proposed ANFIS-MCS framework, it is instructive to consider recent studies that emphasize multi-institutional validation. For example, Li et al. [35] demonstrated that supervised pre-training using clinically interpretable features across diverse datasetsincluding DRISHTI, G1020, ORIGA, and REFUGEcan significantly enhance model generalization. Similarly, Luo et al. [36] introduced the Harvard-GDP dataset, which integrates multimodal imaging data from multiple centers to support both glaucoma detection and progression analysis. These studies underscore the growing emphasis on dataset diversity and cross-institutional benchmarking in the development of clinically robust diagnostic systems. The alignment of our methodology with these broader efforts highlights its potential for future deployment in multi-center screening environments.

The experimental findings directly respond to the core research questions outlined in the Introduction:

- In response to RQ1, the MCS-optimized ANFIS framework achieved superior classification performance, with a test-phase regression coefficient of $R = 0.9832$ and RMSE of 0.0009963, outperforming the PSO-trained counterpart ($R = 0.4811$, RMSE = 0.001723). These results confirm the robustness and adaptability of our hybrid model across real-world fundus images with varying quality and contrast.

- Addressing RQ2, the Gabor-based filtering method, applied to the green channel, successfully extracted retinal vasculature and optic disc edges, resulting in an AUC of 0.90 for vessel segmentation. This demonstrates the effectiveness of the proposed feature extraction strategy in enhancing structural delineation critical to glaucoma detection.

- Regarding RQ3, the performance comparison with PSO demonstrated that MCS yielded a lower final objective function value, faster convergence, and greater classification stability, validating the choice of this metaheuristic for optimizing ANFIS parameters.

Together, these results substantiate the proposed systems clinical potential for assisting in early glaucoma screening and decision support.

4.6   Clinical Relevance and Limitations

The proposed ANFIS-MCS framework demonstrates promising diagnostic performance in glaucoma detection, offering both accuracy and interpretability. By leveraging morphological parameters such as the Cup-to-Disc Ratio (CDR) and Rim-to-Disc Ratio (RDR), the system mimics key clinical reasoning steps used by ophthalmologists, making it a potential candidate for integration into decision-support tools in primary care or screening settings. The fuzzy rule-based nature of the model provides transparency, which can enhance trust and adoption in clinical workflows.

However, this study also has limitations. The dataset used comprises 195 annotated fundus images from a single source, which may not fully capture the variability seen in real-world clinical environments. Additionally, the model was evaluated using internal validation only, without testing on independent external datasets. This limits the generalizability of the findings, and further validation on diverse, multi-center datasets is essential before clinical deployment.

Moreover, the model's performance may be sensitive to the selection of MCS parameters such as population size and discovery rate. While we empirically tuned these settings, a formal sensitivity analysis was not conducted. Although Gabor-based feature extraction enhances vessel and edge detection, the clinical interpretability of these features remains limited compared to more anatomically explicit metrics. Furthermore, the limited dataset may restrict generalizability across different imaging devices, populations, or clinical settings. Future work will aim to evaluate the model on larger, multi-institutional datasets and explore integration with explainable AI techniques to enhance transparency and clinician trust.

Building on these considerations, future efforts will focus on transitioning the MCS-optimized ANFIS framework into a deployable clinical tool. This includes validating the model across larger, multi-institutional

datasets, improving its generalizability to diverse imaging conditions, and ensuring compliance with clinical decision-support standards. Additionally, we plan to integrate explainability features, such as rule-based visual interpretations, to enhance clinician trust and usabilitysimilar to recent approaches in explainable glaucoma detection systems [33]. These steps aim to bridge the gap between algorithmic accuracy and real-world applicability in ophthalmic diagnostics.

Finally, while the proposed ANFIS-MCS framework demonstrated strong performance on the available dataset, it has not yet been tested under real-world clinical conditions. In practice, fundus images often vary in resolution, quality, and acquisition device. These factors can introduce noise and structural variability, potentially affecting model reliability. Future work will focus on validating the system using multi-center, heterogeneous datasets that reflect real clinical environmentsan essential step toward confirming robustness and deployment readiness in ophthalmic screening programs.

5   Conclusion

This study presented a hybrid approach for glaucoma detection and classification using fundus images, combining Gabor-based feature extraction with an Adaptive Neuro-Fuzzy Inference System (ANFIS) optimized through the Modified Cuckoo Search (MCS) algorithm. By extracting meaningful retinal featuresspecifically the cup-to-disc ratio (CDR) and rim-to-disc ratio (RDR)from preprocessed fundus images, the proposed method demonstrated high accuracy in identifying glaucomatous patterns. Performance evaluations showed that the MCS-optimized ANFIS significantly outperformed the traditional PSO in terms of training convergence, prediction accuracy, and robustness on unseen data. The use of Gabor wavelet transformation for vessel segmentation and optic disc localization further enhanced the quality of feature extraction. The resulting classification model achieved an RMSE of 0.0215 and a regression coefficient of 0.9832 on the test set, indicating strong generalization performance. Overall, the results confirm that the proposed system offers an effective and intelligent decision-support tool for early and accurate glaucoma detection, with the potential to aid ophthalmologists in large-scale screening and clinical diagnosis.

Conflict of Interest: "The authors declare no conflict of interest."

References

[1] Blumberg MJ, Varikuti VN, Weiner A. Real-world comparison between the Tonopen and Goldmann applanation tonometry in a university glaucoma clinic. *International Ophthalmology*. 2021; 41: 18151825. DOI: https://doi.org/10.1007/s10792-021-01742-z

[2] Xu J, Li R, Xu H, Yang Y, Zhang S, Ren TL. Recent progress of continuous intraocular pressure monitoring. *Nano Select*. 2022; 3(1): 119. DOI: https://doi.org/10.1002/nano.202100137

[3] Ilesanmi AE, Ilesanmi T, Gbotoso GA. A systematic review of retinal fundus image segmentation and classification methods using convolutional neural networks. *Healthcare Analytics*. 2023; 4: 100261. DOI: https://doi.org/10.1016/j.health.2023.100261

[4] Panda R, N.B Puhan, Panda G. Robust and accurate optic disk localization using vessel symmetry line measure in fundus images. *Biocybernetics and Biomedical Engineering*. 2017; 37(3): 466-476. DOI: https://doi.org/10.1016/j.bbe.2017.05.008

[5] Khan SI, Choubey SB, Choubey A, Bhatt A, Naishadhkumar PV, Basha MM. Automated glaucoma detection from fundus images using wavelet-based denoising and machine learning. *Concurrent Engineering*. 2021; 30(1): 103115. DOI: https://doi.org/10.1177/1063293x211026620

[6] Suot D, Alonso-Caneiro D, Ksieniewicz P, Krzyzanowska-Berkowska P, Iskander DR. Glaucoma classification based on scanning laser ophthalmoscopic images using a deep learning ensemble method. *PLOS ONE.* 2021; 16(6): e0252339. DOI: https://doi.org/10.1371/journal.pone.0252339

[7] Singh LK, Khanna M, Thawkar S. A novel hybrid robust architecture for automatic screening of glaucoma using fundus photos, built on feature selection and machine learningnature driven computing. *Expert Systems.* 2022; 39(10): e13069. DOI: https://doi.org/10.1111/exsy.13069

[8] Pathan S, Kumar P, Pai RM, Bhandary SV. An automated classification framework for glaucoma detection in fundus images using ensemble of dynamic selection methods. *Progress in Artificial Intelligence.* 2023; 12(3): 287301. DOI: https://doi.org/10.1007/s13748-023-00304-x

[9] Feng Y, Li Z, Yang D, Hu H, Guo H, Liu H. Polarformer: Optic disc and cup segmentation using a hybrid CNN-transformer and polar transformation. *Applied Sciences.* 2023; 13(1): 541. DOI: https://doi.org/10.3390/app13010541

[10] Joshi S, Partibane B, Hatamleh WA, Tarazi H, Yadav CS, Krah D. Glaucoma detection using image processing and supervised learning for classification. *Journal of Healthcare Engineering.* 2022; 2022: 2988262. DOI: https://doi.org/10.1155/2022/2988262

[11] Ma F, Li S, Wang S, Guo Y, Wu F, Meng J, Dai C. Deep-learning segmentation method for optical coherence tomography angiography in ophthalmology. *Journal of Biophotonics.* 2024; 17(2): e202300321. DOI: https://doi.org/10.1002/jbio.202300321

[12] Maninis KK, Pont-Tuset J, Arbelez P, Van Gool L. Deep retinal image understanding. In: Ourselin, S., Joskowicz, L., Sabuncu, M., Unal, G., Wells, W. (eds.) *Medical Image Computing and Computer-Assisted Intervention MICCAI 2016: Proceedings Part II, 1721 Oct 2016, Athens, Greece.* Cham: Springer; 2016. p.140148. DOI: https://doi.org/10.1007/978-3-319-46723-8_17

[13] Zilly J, Buhmann JM, Mahapatra D. Glaucoma detection using entropy sampling and ensemble learning for automatic optic cup and disc segmentation. *Computerized Medical Imaging and Graphics.* 2017; 55: 2841. DOI: https://doi.org/10.1016/j.compmedimag.2016.07.012

[14] Tan JH, Acharya UR, Bhandary SV, Chua KC, Sivaprasad S. Segmentation of optic disc, fovea and retinal vasculature using a single convolutional neural network. *Journal of Computational Science.* 2017; 20: 7079. DOI: https://doi.org/10.1016/j.jocs.2017.02.006

[15] Mayee MK, Khanam MH. Simplifying glaucoma diagnosis with U-Net on retinal images. *Traitement du Signal.* 2024; 41(4): 21592168. DOI: https://doi.org/10.18280/ts.410444

[16] Meedeniya D, Shyamalee T, Lim G, Yogarajah P. Glaucoma identification with retinal fundus images using deep learning: Systematic review. *Informatics in Medicine Unlocked.* 2025; 56: 101644. DOI: https://doi.org/10.1016/j.imu.2025.101644

[17] Jang JSR. ANFIS: adaptive-network-based fuzzy inference system. *IEEE Transactions on Systems, Man and Cybernetics.* 1993; 23(3): 665685. DOI: https://doi.org/10.1109/21.256541.

[18] Shyamalee T, Meedeniya D. Attention U-Net for glaucoma identification using fundus image segmentation. In: *Proceedings of the 2022 International Conference on Decision Aid Sciences and Applications (DASA); 2325 Mar 2022, Chiangrai, Thailand.* Piscataway, NJ: IEEE; 2022. p.610. DOI: https://doi.org/10.1109/DASA54658.2022.9765303

[19] Aquino A, Gegndez-Arias ME, Marn D. Detecting the optic disc boundary in digital fundus images using morphological, edge detection, and feature extraction techniques. *IEEE Transactions on Medical Imaging.* 2010; 29(11): 18601869. DOI: https://doi.org/10.1109/TMI.2010.2053042

[20] Lowell J, Hunter A, Steel D, Basu A, Ryder R, Fletcher E, Kennedy L. Optic nerve head segmentation. *IEEE Transactions on Medical Imaging.* 2004; 23(2): 256264. DOI: https://doi.org/10.1109/TMI.2003.823261

[21] Lu S. Accurate and efficient optic disc detection and segmentation by a circular transformation. *IEEE Transactions on Medical Imaging.* 2011; 30(12): 21262133. DOI: https://doi.org/10.1109/TMI.2011.2164261

[22] Shyamalee T, Meedeniya D. CNN based fundus images classification for glaucoma identification. In: *Proceedings of the 2022 2nd International Conference on Advanced Research in Computing (ICARC); 2324 Feb 2022.* Piscataway, NJ: IEEE; 2022. p.200205. DOI: https://doi.org/10.1109/ICARC54489.2022.9754171

[23] Diaz-Pinto A, Morales S, Naranjo V, Khler T, Mossi JM, Navea A. CNNs for automatic glaucoma assessment using fundus images: an extensive validation. *BioMedical Engineering OnLine.* 2019; 18(29). DOI: https://doi.org/10.1186/s12938-019-0649-y

[24] Asaoka R, Tanito M, Shibata N, Mitsuhashi K, Nakahara K, Fujino Y, et al. Validation of a deep learning model to screen for glaucoma using images from different fundus cameras and data augmentation. *Ophthalmology Glaucoma.* 2019; 2(4): 224231. DOI: https://doi.org/10.1016/j.ogla.2019.03.008

[25] Shyamalee T, Meedeniya D. Glaucoma Detection with Retinal Fundus Images Using Segmentation and Classification. *Machine Intelligence Research.* 2022; 19(6): 563580. DOI: https://doi.org/10.1007/s11633-022-1354-z

[26] Cheng J, Liu J, Xu Y, Yin F, Wong DWK, Tan NM, Tao D, Cheng CY, Aung T, Wong TY. Superpixel classification based optic disc and optic cup segmentation for glaucoma screening. *IEEE Transactions on Medical Imaging.* 2013; 32(6): 10191032. DOI: https://doi.org/10.1109/TMI.2013.2247770

[27] Fu H, Cheng J, Xu Y, Zhang C, Wong DWK, Liu J, Cao X. Disc-aware ensemble network for glaucoma screening from fundus image. *IEEE Transactions on Medical Imaging.* 2018; 37(11): 24932501. DOI: https://doi.org/10.1109/TMI.2018.2837012

[28] Almazroa A, Alodhayb S, Osman E, Ramadan E, Hummadi M, Dlaim M, Alkatee M, Raahemifar K, Lakshminarayanan V. Retinal fundus images for glaucoma analysis: the RIGA dataset. In: Medical Imaging 2018: Imaging Informatics for Healthcare, Research, and Applications. Proc. SPIE 10579; 2018 Mar 6. p.105790B. DOI: https://doi.org/10.1117/12.2293584

[29] Martinez-Perez ME, Witt N, Parker KH, Hughes AD, Thom SA. Automatic optic disc detection in colour fundus images by means of multispectral analysis and information content. *PeerJ.* 2019; 7: e7119. DOI: https://doi.org/10.7717/peerj.7119.

[30] Yang XS, Suash D. Cuckoo search via Lvy flights. In: *2009 World Congress on Nature & Biologically Inspired Computing (NaBIC)*; 2009 Dec 911. pp. 210214. DOI: https://doi.org/10.1109/NABIC.2009.5393690.

[31] Soares JVB, Leandro JJG, Cesar RM Jr, Jelinek HF, Cree MJ. Retinal vessel segmentation using the 2-D Gabor wavelet and supervised classification. *IEEE Transactions on Medical Imaging.* 2006; 25(9): 12141222. DOI: https://doi.org/10.1109/TMI.2006.879967.

[32] Kumar JRH, Seelamantula CS, Kamath YS, Jampala R. Rim-to-disc ratio outperforms cup-to-disc ratio for glaucoma prescreening. *Scientific Reports.* 2019; 9: 7099. DOI: https://doi.org/10.1038/s41598-019-43385-2.

[33] Shyamalee T, Meedeniya D, Lim G, Karunarathne M. Automated tool support for glaucoma identification with explainability using fundus images. *IEEE Access.* 2024; 12: 1729017307. DOI: https://doi.org/10.1109/ACCESS.2024.3359698.

[34] Das D, Nayak DR. GS-Net: Global self-attention guided CNN for multi-stage glaucoma classification. In: *2023 IEEE International Conference on Image Processing (ICIP)*; 811 Oct 2023. p.34543458. DOI: https://doi.org/10.1109/ICIP49359.2023.10222689.

[35] Li Y, Carrillo-Perez F, Owaifeer AM, Alawad M, Gevaert O. Enhancing glaucoma detection through supervised pre-training with intermediate phenotypes: A multi-institutional study. *medRxiv* [Preprint] 2025. DOI: https://doi.org/10.1101/2025.04.22.25326210.

[36] Luo Y, Shi M, Tian Y, Elze T, Wang M. Harvard glaucoma detection and progression: A multimodal multitask dataset and generalization-reinforced semi-supervised learning. In: *2023 IEEE/CVF International Conference on Computer Vision (ICCV)*; 1-6 Oct 2023. p.2041420425. DOI: https://doi.org/10.1109/ICCV51070.2023.01872.

Asma Naseri
Department of Electrical and Biomedical Engineering
University of Bojnord
Bojnord, Iran
E-mail: asmanaseri58@gmail.com

Ali Khazaee
Department of Electrical and Biomedical Engineering
Assistant Professor of Electrical Engineering
University of Bojnord
Bojnord, Iran
E-mail: khazaee.a@gmail.com